JPn Neuroscience
The Journal of Physiology

Carbachol excites sublaterodorsal nucleus neurons projecting to the spinal cord

F. J. Weng, R. H. Williams, J. M. Hawryluk, J. Lu, T. E. Scammell, C. B. Saper and E. Arrigoni

Department of Neurology, Beth Israel Deaconess Medical Center, Boston, MA 02215, USA

Key points

- Activation of spinally projecting sublaterodorsal nucleus (SLD) neurons inhibits motor activity, in part through spinal inhibitory interneurons, to produce muscle atonia during rapid-eye-movement (REM) sleep.
- It has long been hypothesized that acetylcholine released during REM sleep contributes to REM sleep atonia through activation of SLD neurons.
- We show, using whole-cell recordings in brainstem slices, that acetylcholine directly excites spinally projecting SLD neurons via M_1 and M_3 muscarinic receptors, and increases afferent excitatory synaptic input to these neurons.
- These results suggest that acetylcholine contributes to REM sleep muscle atonia through excitation of spinally projecting SLD neurons.

Abstract Considerable electrophysiological and pharmacological evidence has long suggested an important role for acetylcholine in the regulation of rapid-eye-movement (REM) sleep. For example, injection of the cholinergic agonist carbachol into the dorsomedial pons produces an REM sleep-like state with muscle atonia and cortical activation, both of which are cardinal features of REM sleep. Located within this region of the pons is the sublaterodorsal nucleus (SLD), a structure thought to be both necessary and sufficient for generating REM sleep muscle atonia. Subsets of glutamatergic SLD neurons potently contribute to motor inhibition during REM sleep through descending projections to motor-related glycinergic/GABAergic neurons in the spinal cord and ventromedial medulla. Prior electrophysiological and pharmacological studies examining the effects of acetylcholine on SLD neurons have, however, produced conflicting results. In the present study, we sought to clarify how acetylcholine influences the activity of spinally projecting SLD (SLDsp) neurons. We used retrograde tracing in combination with patch-clamp recordings and recorded pre- and postsynaptic effects of carbachol on SLDsp neurons. Carbachol acted presynaptically by increasing the frequency of glutamatergic miniature excitatory post-synaptic currents. We also found that carbachol directly excited SLDsp neurons by activating an Na^+–Ca^{2+} exchanger. Both pre- and postsynaptic effects were mediated by co-activation of M_1 and M_3 muscarinic receptors. These observations suggest that acetylcholine produces synergistic, excitatory pre- and postsynaptic responses on SLDsp neurons that, in turn, probably serve to promote muscle atonia during REM sleep.

(Received 10 July 2013; accepted after revision 12 December 2013; first published online 16 December 2013)
Corresponding author E. Arrigoni: Department of Neurology, Beth Israel Deaconess Medical Center, 3 Blackfan Circle, Center for Life Science Room 713, Boston, MA 02215, USA. Email: earrigon@bidmc.harvard.edu

Abbreviations 4-DAMP, 1,1-Dimethyl-4-diphenylacetoxypiperidinium iodide; ACSF, artificial cerebrospinal fluid; BAPTA, 1,2-bis-(o-aminophen-oxy)ethane-N,N,N′,N′-tetraacetic acid; C6, hexamethonium chloride; DHβE, dihydro-β-erythroidine hydrobromide; E_{NCX}, Na^+–Ca^{2+} exchanger reversal potential; I_h, hyperpolarization-activated current; *I–V*, current–voltage relationship; LC, locus coeruleus; MEC, mecamylamine; mEPSC, miniature excitatory postsynaptic current; MLA, methyllycaconitine citrate; peri-LCα, peri-locus coeruleus-α; REM, rapid eye movement; sEPSC, spontaneous excitatory postsynaptic currents; SLD, sublaterodorsal nucleus; SLDsp, spinally projecting sub-laterodorsal neurons; TH, tyrosine hydroxylase; TTX, tetrodotoxin; V_h, holding potential

DOI: 10.1113/jphysiol.2013.261800

Introduction

During rapid-eye-movement (REM) sleep, skeletal muscle tone, with the exception of those muscles related to breathing and eye movements, is dramatically reduced. Thus, skeletal muscle atonia is a defining feature of REM sleep. Dysfunction or damage to the supraspinal circuitry regulating REM sleep motor atonia, such as occurs in REM sleep behaviour disorder, results in the appearance of dream-enactment behaviour (Gagnon *et al.* 2006). Conversely, inappropriate activation of the supraspinal circuitry regulating REM sleep motor atonia, such as occurs in narcolepsy with cataplexy, results in sudden episodes of muscle atonia during wakefulness (Scammell, 2003). A more detailed understanding of the supraspinal circuitry regulating REM muscle atonia would provide not only important details of the neurobiology of REM sleep but probably also the pathophysiological bases of REM sleep behaviour disorder and cataplexy.

The sublaterodorsal nucleus (SLD) contains neurons that are crucial for the generation of atonia during REM sleep (Fuller *et al.* 2007; Luppi *et al.* 2012). In rats and mice, the SLD is located in the dorsal pons immediately ventral to the caudal laterodorsal tegmental nucleus and the locus coeruleus (LC; Franklin & Paxinos, 1997; Clement *et al.* 2011). This region is also known as the subcoeruleus area and is likely to be the homologue of the cat peri-locus coeruleus-α (peri-LCα; Sakai *et al.* 2001). Considerable evidence suggests that the SLD is both necessary and sufficient for driving muscle atonia during REM sleep (Sakai *et al.* 2001; Boissard *et al.* 2002; Lu *et al.* 2006; Fuller *et al.* 2007; Luppi *et al.* 2011; Vetrivelan *et al.* 2011). Pharmacological activation of putative SLD neurons in cats and rats rapidly produces an REM sleep-like state that is characterized by muscle atonia and cortical activation, with prominent EEG theta activity (Lai & Siegel, 1991; Onoe & Sakai, 1995; Boissard *et al.* 2002). Electrical stimulation of the SLD region in rats produces bilateral or contralateral suppression of muscle tone, depending on the site of the stimulation (Hajnik *et al.* 2000). Furthermore, small lesions of this area in cats or rats or focal disruption of glutamatergic transmission in these neurons in mice produces REM sleep without atonia, which is phenotypically very similar to that seen in humans with REM sleep behaviour disorder (Morrison, 1988; Lu *et al.* 2006; Krenzer *et al.* 2011). Interestingly, degeneration of the SLD neurons in humans is hypothesized to be a major component of the pathogenesis of human REM sleep behaviour disorder (Boeve *et al.* 2007; Mathis *et al.* 2007).

Sublaterodorsal nucleus neurons are glutamatergic, active during REM sleep (Lu *et al.* 2006; Clement *et al.* 2011; Krenzer *et al.* 2011), and are thought to promote atonia through descending projections that couple synaptically with glycinergic/GABAergic premotor neurons in the spinal cord or ventromedial medulla (Soja *et al.* 1991; Boissard *et al.* 2002; Lu *et al.* 2006; Fuller *et al.* 2007; Lai *et al.* 2010; Krenzer *et al.* 2011; Vetrivelan *et al.* 2011; Chase, 2013). During REM sleep, acetylcholine is thought to participate in the activation of these descending atonia pathways (Jones, 1991; McCarley, 2007). For example, when the cholinergic agonist carbachol is injected in the vicinity of the SLD in rats and, to a lesser extent, in mice, an REM sleep-like state, including muscle atonia, EEG desynchronization, rapid eye movements and ponto-geniculate waves, is induced (Baghdoyan, 1997; Kubin, 2001). The cat SLD has also been shown to contain REM sleep-on neurons that are activated by carbachol (Sakai & Koyama, 1996; Sakai *et al.* 2001). Although researchers have identified several sites in the medial pontine reticular formation at which carbachol can elicit these REM sleep-like phenomena, the SLD region is the most effective site (Kubin, 2001). Accordingly, the cat SLD has been shown to contain REM sleep-on neurons that are activated by carbachol (Sakai & Koyama, 1996; Sakai *et al.* 2001).

It has been a major challenge to identify SLD neurons that are active during atonia in an *in vitro* brain slice preparation. A particular challenge derives from the fact that the SLD region is heterogeneous and includes neurons with no established relationship to REM sleep atonia. This heterogeneity may explain why previous electrophysiological studies of SLD region neurons have found both excitatory and inhibitory responses to carbachol (Sakai & Koyama, 1996; Brown *et al.* 2006; Garcia-Rill *et al.* 2007; Heister *et al.* 2009). In an effort to reconcile these conflicting reports, we developed a novel approach to help clarify the following two key issues. (i) How does carbachol affect SLD neurons that subserve REM sleep atonia? (ii) Does carbachol act directly on these neurons or indirectly through local or distant circuitry? Our experimental approach comprised a combination of retrograde tracing and *in vitro* electrophysiology techniques that facilitated the identification of spinally projecting SLD (SLDsp) neurons and subsequent characterization of the specific cellular mechanisms by which carbachol excites SLDsp neurons (Lu *et al.* 2006; Krenzer *et al.* 2011).

Methods

Animal care and ethical approval

We used 103 C57BL/6 male and female mice, between the ages of 9 and 25 days (The Jackson Laboratory, Bar Harbor, ME, USA). The mice were housed in a pathogen-free barrier animal research facility maintained on a 12 h–12 h light–dark cycle (lights on at 07.00 h) at 22°C ambient temperature and with *ad libitum* access to food and water. Care of the mice met the National Institutes of Health

standards, as set forth in the *Guide for the Care and Use of Laboratory Animals*, published by the US National Institutes of Health (NIH publication no. 85-23, revised 1996), and all protocols were approved by the Beth Israel Deaconess Medical Center Institutional Animal Care and Use Committee.

Fluorescent retrograde labelling of SLD neurons

We injected rhodamine-labelled fluorescent latex beads (~0.1 μm diameter; Lumafluor Inc., Naples, FL, USA) into the ventral horn of the spinal cord. These beads are taken up by nerve terminals and retrogradely transported. We initially anaesthetized the mice in an induction chamber with isoflurane (4–5% in oxygen, using an anaesthetic vapourizer). We then fixed the mouse in a stereotaxic frame and reduced the dose of isoflurane to 1–2%. We incised the skin over the spine and, after appropriate dissection and laminectomy, we lowered a glass micropipette vertically into the spinal cord to the designated co-ordinate. To minimize injury to the spinal cord, we slowly injected 150 nl of beads over 5 min using a silane-coated glass micropipette (25–30 μm tip diameter) and an air-pressure injection system. The injections were targeted at laminae VII and VIII at the T1 level (mediolateral, +0.4 mm and dorsoventral, −0.5 mm; Franklin & Paxinos, 1997). In these experiments, we used only mice in which the injection was placed in the ventral horn. Injections into the dorsal horn retrogradely labelled the LC but not the SLD, so we excluded mice with labelling restricted to the LC and mice in which the injection was restricted to the dorsal horn. Two to five days after the surgery, we used the injected mice to prepare brain slices for *in vitro* recordings. We found many retrogradely labelled SLD neurons ipsilateral and contralateral to the injection, and we recorded neurons from either side of the pons.

Slice preparation and whole-cell patch-clamp recordings

To prepare brain slices, we anaesthetized mice with isoflurane to the point of respiratory arrest, followed by decapitation. Using a vibrating microtome (VT1000; Leica, Bannockburn, IL, USA), we cut coronal brain slices (300 μm thick) in ice-cold artificial cerebral spinal fluid (ACSF; Hepes-buffered solution) oxygenated with 100% O_2. We recorded the slices submerged and perfused (2 ml min^{-1}) with ACSF. We recorded only retrogradely labelled neurons (containing the fluorescent beads) in the SLD region in two or three coronal slices (−4.9 to −5.5 mm from bregma; Franklin & Paxinos, 1997; Figs 1 and 2). To guide our recordings, we used fluorescence and infrared differential interference contrast video microscopy using a fixed stage upright microscope (BX51WI; Olympus America Inc.) equipped with a Nomarski water immersion lens (×40/0.8 W) and infrared-sensitive CCD cameras (300T-RC; DAGE MTI, Michigan City, IN, USA; or ORCA-ER; Hamamatsu, Bridgewater, NJ, USA). We recorded in whole-cell configuration at room temperature using a Multiclamp 700B amplifier (Molecular Devices, Foster City, CA, USA), a Digidata 1322A interface and Clampex 9.0 software (Molecular Devices). We monitored the series resistance at regular intervals, and we discarded the data if neurons showed an unstable resting membrane potential or if the series resistance changed by more than 25%.

Data analysis and statistics

We analysed the current-clamp and voltage-clamp recordings using Clampfit 9.0 (Molecular Devices) and IGOR Pro 6 (WaveMetrics, Lake Oswego, OR, USA). We measured the resting membrane potential in control ACSF and in SLDsp neurons that exhibited spontaneous firing below 2.5 Hz. We calculated input resistance before and during carbachol application using 500 ms hyperpolarizing current pulses in tetrodotoxin (TTX) and at resting membrane potential. We calculated the action potential amplitude as the voltage between the threshold and the action potential peak. We calculated the action potential duration as the width at the voltage halfway between the action potential threshold and the action potential peak. We determined the action potential threshold as the voltage at which the slope of the action potential reached ≥ 20 V s^{-1}. We calculated the predicted Na^+–Ca^{2+} exchanger reversal potential (E_{NCX}) for a 3:1 stoichiometry as $E_{NCX} = 3E_{Na} - 2E_{Ca}$ (Weber *et al.* 2002). We analysed the spontaneous and miniature excitatory postsynaptic currents (sEPSCs and mEPSCs) offline using Mini Analysis 6 (Synaptosoft, Leonia, NJ, USA). We ranked the synaptic events (5 min in control conditions, the last 5 min of 10 min carbachol application, and the last 5 min of a 15 min washout) by amplitude and interevent interval to prepare cumulative probability distributions. We compared the results using the non-parametric Kolmogorov–Smirnov test. For all the statistical analyses, we used StatView (SAS Institute, Cary, NC, USA). We normalized all the values by dividing the values of control and treatment samples by the mean of the control sample. Such normalization conserves the distribution and the relative variance of the samples, allowing the subsequent use of Student's t test. We used Student's paired t tests or one-way ANOVA (with repeated measures) followed by Fisher's PLSD tests for statistical analysis. A value of $\alpha < 0.05$ was considered significant. Results are expressed as means ± SEM.

Reagents and solutions

The composition of the ACSF was as follows (mM): 140 NaCl, 3 KCl, 1.3 $MgSO_4$, 2.4 $CaCl_2$, 1.4 NaH_2PO_4, 11 glucose and 5 Hepes (pH adjusted to 7.2 with NaOH, 315–320 mosmol l^{-1}). The pipette solution was as follows (mM): 120 potassium gluconate, 10 KCl, 3 $MgCl_2$, 10 Hepes, 2.5 potassium ATP, 0.5 sodium GTP and 0.1 Alexa Fluor 555 hydrazide fluorescence dye (Invitrogen Co., Carlsbad, CA, USA; pH adjusted to 7.2 with KOH; 280 mosmol l^{-1}). We recorded mEPSCs in TTX (1 μM). For recordings in extracellular low Na^+, we used a choline-based solution in which 80% of the NaCl was replaced with choline chloride and a pipette solution in which we replaced 10 mM potassium gluconate with 10 mM NaCl (final concentration 110 mM potassium gluconate). We purchased TTX, KB-R7943 mesylate, dihydro-β-erythroidine hydrobromide (DHβE), 4-DAMP, AQ-RA-741, PD102807, VU0255035 and J104129 from Tocris Bioscience (Ellisville, MO, USA). We purchased all the other reagents from Sigma-Aldrich (St Louis, MO, USA). We dissolved KB-R7943 mesylate, 4-DAMP, AQ-RA-741, PD102807, VU0255035 and J104129 in dimethyl sulfoxide. The final concentration of dimethyl sulfoxide in the ACSF was $<0.1\%$.

Histology

Immediately after the preparation of brain slices, we removed the spinal cords, fixed them overnight in 10% buffered formalin (Fisher Scientific, Pittsburg, PA, USA), then cut them into 80 μm axial sections on a freezing microtome and examined them with fluorescence microscopy to validate the location of the injected beads.

After the slice recordings, we fixed the brain slices (300 μm) overnight in 10% buffered formalin. We photographed the brain slices under fluorescence microscopy to document the location of retrogradely labelled neurons. To identify the recorded neurons filled with the red/orange fluorescent dye (Alexa Fluor 555) we dissolved the beads in xylene. We dehydrated the recorded slices in a series of graded ethanols (50, 70, 95 and 100%; 10 min for each solution) and then placed the slices in xylene for 10 min. This technique thoroughly dissolved the beads, and we then photographed the slice. By digitally superimposing the two images, we mapped the location of the recorded neurons in relationship to the cluster of retrogradely labelled cells in the SLD.

Next, we resectioned the recorded slices into 60 μm sections on a freezing microtome and then processed them for tyrosine hydroxylase (TH) immunoreactivity. We incubated the sections overnight in rabbit TH primary antibody (1:1000 dilution; AB152; lot JC1634159; Chemicon International/Millipore, Temecula, CA, USA) in PBS containing 0.3% Triton X-100 and then the next day in goat Cy2-anti-rabbit IgG secondary antibody (1:500 dilution in PBS containing 0.3% Triton X-100; Jackson ImmunoResearch, West Grove, PA, USA) for 2 h. This rabbit polyclonal antibody is raised against purified rat pheochromacytoma TH. It recognizes a single band of 62 kDa molecular weight on Western blots of rat brain (manufacturer) and stains a pattern of neurons in the rat pons consistent with previous reports (Bruinstroop *et al.* 2011). Omission of the TH primary antisera showed no immunoreactivity above background. We mounted the sections on gelatin-coated slices, dehydrated them in ascending concentrations of ethanol, delipidated in xylene and coverslipped them. We examined the sections under fluorescence to determine the location of the recorded neurons with respect to the TH-labelled neurons of the LC and whether or not they were positive for TH immunoreactivity.

Results

Recordings from REM-atonia neurons of the SLD in brainstem *in vitro* slices

To facilitate the identification of SLDsp neurons in our *in vitro* brainstem slice preparation, we injected fluorescent latex microspheres (which are physiologically inert) into the ventral horn of the spinal cord *in vivo* (Fig. 1). Two to five days later, the mice were killed for *in vitro* recordings. We recorded only from retrogradely labelled SLD neurons containing the fluorescent microspheres (Figs 1 and 2). The LC, which is immediately dorsal to the SLD, also projects to the spinal cord (VanderHorst & Ulfhake, 2006; Bruinstroop *et al.* 2011). To avoid any spinally projecting LC neurons, we focused our analysis on neurons that were located ventral to the LC and dorsal to the trigeminal motor nucleus, positive for microspheres but lacking TH immunoreactivity (determined *post hoc*).

We found that the SLDsp neurons were a relatively homogeneous population with electrophysiological properties distinct from the neighbouring noradrenergic LC neurons. The SLDsp neurons had an average membrane potential of -41.2 ± 0.8 mV and an average input resistance of 597 ± 51 MΩ ($n = 32$). Seventy-seven per cent of SLDsp neurons were spontaneously active ($n = 65$ in which spontaneous firing was assessed). These spontaneously active SLDsp neurons had a mean firing frequency of 3.0 ± 0.3 Hz ($n = 50$) and a mean firing threshold of 47.3 ± 0.6 mV ($n = 10$). The SLDsp neurons had a relatively narrow action potential (1.91 ± 0.09 ms, $n = 50$) compared with LC neurons (2.80 ± 0.19 ms, $n = 9$; $P < 0.01$; Student's unpaired t test) and had an after-hyperpolarization amplitude of -15.2 ± 0.8 mV ($n = 13$). In contrast to LC neurons, SLDsp neurons showed little or no delay in rebound firing during

repolarization from hyperpolarizing potentials (SLDsp neurons, 151.6 ± 23.3 ms, $n = 24$ *vs.* LC neurons, 685.5 ± 108.7 ms, $n = 9$; $P < 0.01$; Student's unpaired *t* test). In addition, they lacked low-threshold Ca^{2+} spikes and had an inwardly rectifying K^+ current and little or no hyperpolarization-activated current (I_h). These firing characteristics are similar to those of a previously described population in this region (Brown *et al.* 2006), although their spinal projections were not known at the time.

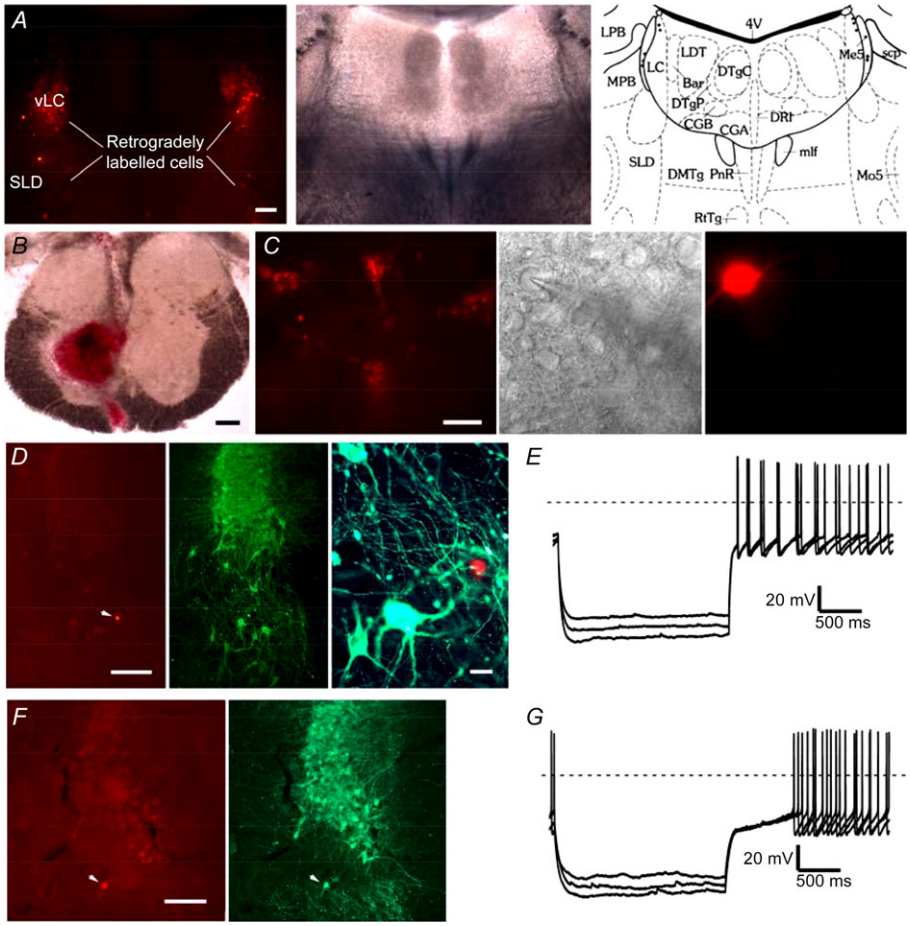

Figure 1. Whole-cell recordings in brainstem slices of spinally projecting sublaterodorsal (SLDsp) neurons

A, photographs show the distribution of fluorescent retrogradely labelled neurons in the ventral locus coeruleus (vLC) and sublaterodorsal nucleus (SLD; left), the same section visualized under bright field illumination (centre) and represented as a schematic drawing of the nuclei, 4th ventricle (4V); Barrington's nucleus (Bar); central gray, alpha part (CGA); central gray, beta part (CGB); dorsomedial tegmental area (DMTg); dorsal raphe nucleus, interfascicular (DRI); dorsal tegmental nucleus central (DTgC); dorsal tegmental nucleus pericentral (DTgP); locus coeruleus (LC); laterodorsal tegmental nucleus (LDT); lateral parabrachial nucleus (LPB); mesencephalic 5 nucleus (Me5); medial longitudinal fasciculus (mlf); medial parabrachial nucleus (MPB); motor trigeminal nucleus (Mo5); pontine raphe nucleus (PnR); reticulotegmental nucleus of pons (RtTg); superior cerebellar peduncle (scp); sublaterodorsal nucleus (SLD); (adapted from Franklin & Paxinos, 1997; scale bar = 200 μm). *B*, the injection site in the T1 ventral horn (scale bar = 200 μm). *C*, an example of recordings of SLDsp neurons visualized under fluorescent and infrared differential interference contrast systems and after being filled with Alexa Fluor 555 from the recording pipette (scale bar = 20 μm). *D*, an example of a recorded SLDsp neuron, filled with Alexa Fluor 555 (left), located immediately ventral to the locus coeruleus (LC), and negative for tyrosine hydroxylase (TH) immunoreactivity (in green; centre panel, scale bar = 200 μm; right panel, scale bar = 20 μm). *E*, the firing of SLDsp neurons is characterized by a small delay or no delay in rebound firing during repolarization from hyperpolarizing potentials, no low-threshold Ca^{2+} spikes, and little or no hyperpolarization-activated current (I_h)-mediated depolarizing sag. *F* and *G*, an example of a recorded neuron that was retrogradely labelled from the spinal cord, that was located ventral of the LC but was positive for TH immunoreactivity (Alexa Fluor 555 in red and TH immunoreactivity in green; scale bar = 200 μm). This SLD TH-positive spinally projecting neuron has the electrophysiological properties of a typical LC neuron, including delayed rebound firing on recovery from hyperpolarizing current pulses due to activation of an A-type current and no I_h-mediated depolarizing sag.

Carbachol excites SLDsp neurons through M_1 and M_3 muscarinic receptors

We found that carbachol (15 μM) excites 83% of SLDsp neurons. Of 54 SLDsp neurons tested, only six were inhibited and three showed no response. In current-clamp recordings of SLDsp neurons that were excited, carbachol induced membrane depolarization (+6.1 ± 0.4 mV; $n = 7$) and increased the spontaneous firing rate (by 100.8 ± 25.3%; $n = 8$; $P < 0.01$, Student's paired t test, carbachol *vs.* control conditions; Fig. 2). These effects were not associated with a change in input resistance (control conditions, 525 ± 61 MΩ and carbachol, 507 ± 61 MΩ; $n = 10$; $P = 0.54$, Student's paired t test, carbachol *vs.* control conditions). In addition, carbachol did not change the action potential amplitude (control conditions, 58.0 ± 4.0 mV and carbachol, 57.1 ± 3.9 mV; $n = 9$; $P > 0.05$, Student's paired t test, carbachol *vs.* control conditions), duration (control conditions 1.78 ± 0.16 ms and carbachol, 1.81 ± 0.16 ms; $n = 9$; $P > 0.05$, Student's paired t test, carbachol *vs.* control conditions) and action potential threshold (control conditions, −30.1 ± 1.8 mV and carbachol, −29.2 ± 1.9 mV; $n = 9$; $P > 0.05$, Student's paired t test, carbachol *vs.* control conditions).

In voltage-clamp recordings [holding potential (V_h) = −60 mV] from SLDsp neurons excited by carbachol, carbachol evoked an inward current (−20.1 ± 5.2 pA; $n = 12$; $P < 0.01$, Student's paired t test, carbachol *vs.* control conditions) accompanied by an increase in membrane current noise. These effects were maintained in the presence of 1 μM TTX (−20.6 ± 2.2 pA; $n = 22$; $P < 0.01$, Student's paired t test, carbachol *vs.* control conditions). The carbachol-mediated current was unaffected by a cocktail of nicotinic receptor antagonists, i.e. hexamethonium chloride (C6; 100 μM) plus methyllycaconitine citrate (MLA; 10 nM) plus mecamylamine (MEC; 1 μM) plus dihydro-β-erythroidine hydrobromide (DHβE; 500 nM), but was abolished by the muscarinic receptor antagonist scopolamine (10 μM), indicating that carbachol directly excites SLDsp neurons through muscarinic receptors (Fig. 3). In the presence of the nicotinic receptor antagonists, carbachol still evoked an inward current of comparable amplitude to that in control ACSF (−19.8 ± 3.6 pA; $n = 7$; $P < 0.01$, Student's paired t test, carbachol + C6 + MLA + MEC + DHβE *vs.* C6 + MLA + MEC + DHβE), but not in the presence of scopolamine (−2.9 ± 0.8 pA; $n = 9$; $P > 0.05$, Student's paired t test, carbachol + scopolamine *vs.* scopolamine). Application of pirenzepine, an preferential M_1 receptor antagonist, or 1,1-Dimethyl-4-diphenylacetoxypiperidinium iodide (4-DAMP), a preferential M_3/M_1 receptor antagonist, both reduced the response of carbachol. Pirenzepine (10 μM) reduced the carbachol-mediated current to 23.3 ± 7.6% ($n = 8$), whereas 4-DAMP (100 nM) reduced it to 43.8 ± 9.1% ($n = 12$). It is known that pirenzepine also binds with relative high affinity to M_3 and M_4 receptors, although it has much lower affinity for M_2 (Buckley *et al.* 1989). It is unclear whether 10 μM pirenzepine can antagonize the carbachol response at M_3 receptors. For instance, it antagonizes ligand-induced responses at M_3 receptors in submaxillary gland membranes but not in subthalamic neurons (Buckley *et al.* 1989; Shen & Johnson, 2000). Therefore, based on our results with pirenzepine and 4-DAMP, we concluded that M_1 receptors are likely to mediate arbachol excitation of SLDsp neurons, but the involvement of the M_3 subtype was still uncertain. Combined application of pirenzepine and 4-DAMP (10 μM pirenzepine + 100 nM 4-DAMP) abolished the carbachol-evoked inward current (−1.3 ± 0.6 pA; $n = 6$; $P > 0.05$, Student's paired t test, carbachol + pirenzepine + 4-DAMP *vs.* pirenzepine + 4-DAMP), whereas combined application of the preferential M_2/M_4 receptor antagonist AQ-RA-741 and the M_4-selective receptor antagonist PD102807 (AQ-RA-741 200 nM + PD102807 1 μM) was ineffective in antagonizing the carbachol-evoked inward current (−22.3 ± 3.1 pA; $n = 7$; $P < 0.01$, Student's paired t test, carbachol + AQ-RA-741 + PD102807 *vs.* AQ-RA-741 + PD102807). Therefore, and in agreement with the excitatory response on SLDsp neurons, we concluded that carbachol acts through M_1 and/or M_3 receptor subtypes (G_q-coupled receptors) but not through M_2 and M_4 subtypes (G_i-coupled receptors). We next used two selective antagonists for M_1 and M_3 receptors, namely VU0255035 (M_1– selective; Sheffler *et al.* 2009) and J104129 (M_3–selective; Mitsuya *et al.* 1999). We found that both reduced the response of carbachol but did not abolish it. VU0255035 (1 μM) reduced the carbachol-mediated current to 56.1 ± 17.8% ($n = 7$) and J104129 (50 nM)

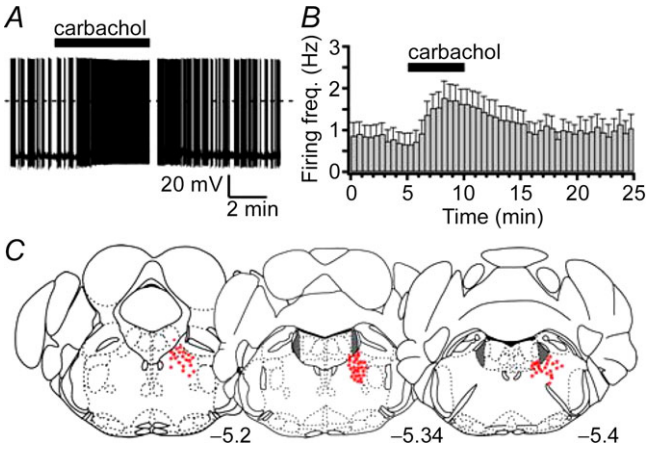

Figure 2. Carbachol excites SLDsp neurons
A, the response of a typical SLDsp neuron to carbachol (15 μM). *B*, a 5 min application of carbachol increases the firing frequency of eight SLDsp neurons. *C*, the distribution of 72 recorded SLDsp neurons. The LC is highlighted in grey. The numbers at the bottom indicate the distance (in millimetres) posterior to bregma.

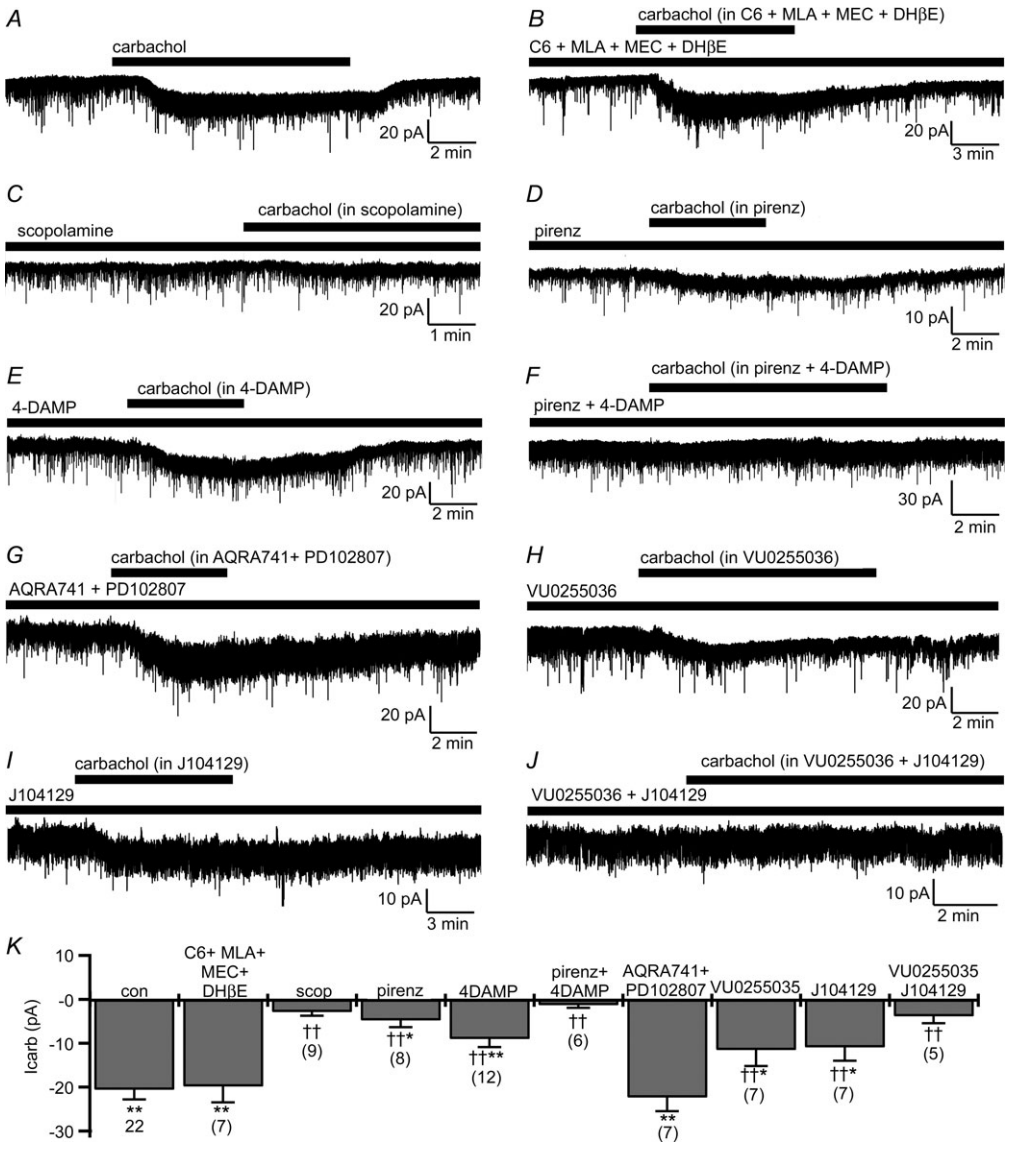

Figure 3. Carbachol excites the SLDsp neurons through M_1 and M_3 muscarinic receptors
A–C, carbachol (15 μM) activates an inward current (*A*) that is unaffected by the following cocktail of nicotinic receptor antagonists: hexamethonium chloride (C6; 100 μM) + methyllycaconitine citrate (MLA; 10 nM) + mecamylamine (MEC; 1 μM) + dihydro-β-erythroidine hydrobromide (DHβE; 500 nM; *B*), but is blocked by the muscarinic receptor antagonist, scopolamine (10 μM; *C*). *D–F*, the preferential M_1 receptor antagonist pirenzepine (10 μM; *D*) and the preferential M_3/M_1 receptor antagonist 1,1-Dimethyl-4-diphenylacetoxypiperidinium iodide (4-DAMP; 100 nM; *E*) only produce a partial block of the carbachol-mediated current, whereas, when co-applied (pirenzepine + 4-DAMP) they abolish the effects of carbachol (*F*). *G*, combined application of the preferential M_2/M_4 receptor antagonist AQ-RA-741 (200 nM) and the M_4-selective receptor antagonist PD102807 (1 μM) does not block carbachol-evoked inward current. *H–J*, both the M_1-selective antagonist VU0255035 (1 μM; *H*) and the M_3-selective antagonist J104129 (50 nM; *I*) only produce a partial block of the response of carbachol, but when co-applied (VU0255035 + J104129) they abolish the effects of carbachol (*J*). *K*, summary histogram of carbachol-mediated current recorded in control artificial cerebrospinal fluid (ACSF; con; $n = 22$) and in the presence of C6 + MLA + MEC + DHβE ($n = 7$), of scopolamine (scop; $n = 9$), of pirenzepine (pirenz; $n = 8$), of 4-DAMP ($n = 12$), of pirenzepine + 4-DAMP ($n = 6$), of AQ-RA-741 + PD102807 ($n = 7$), of U0255035 ($n = 7$), of J104129 ($n = 7$) and of VU0255035 + J104129 ($n = 5$). $^*P < 0.05$ and $^{**}P < 0.01$, Student's paired *t* test, comparing holding currents before and during carbachol applications in the different conditions. †$P < 0.05$, ††$P < 0.01$, $F_{(9,80)} = 9.068$, $P < 0.001$, one-way ANOVA, Fisher's PLSD, comparing carbachol-mediated current in control ACSF (con) *vs.* the carbachol-mediated current of the pharmacologically treated groups (C6 + MLA + MEC + DHβE, scop, pirenz, 4DAMP, pirenz + 4DAMP, AQRA741 + PD102807, VU0255035, J104129 and VU0255035 + J104129). All recordings were conducted in TTX (1 μM) and at a holding potential (V_h) of −60 mV.

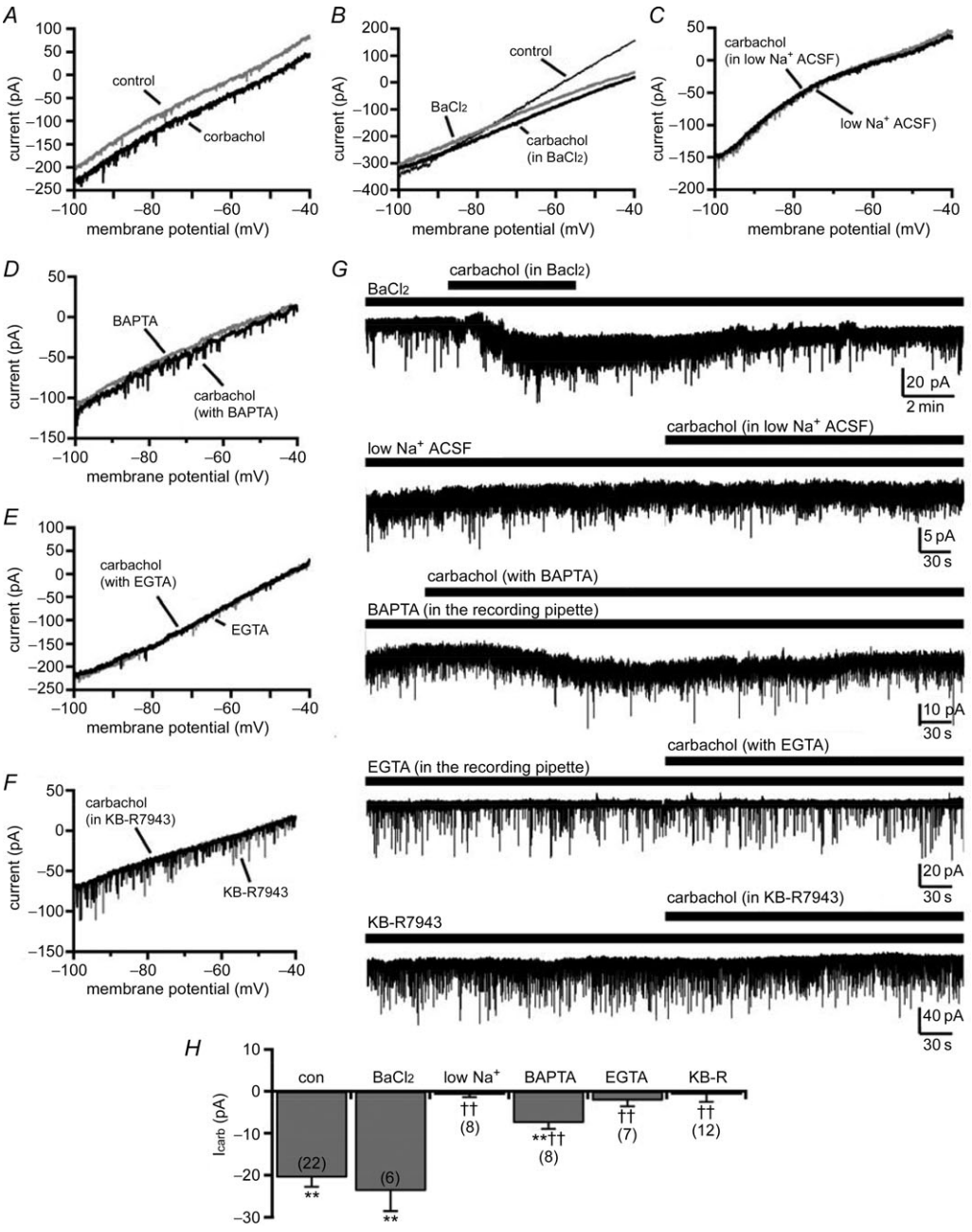

Figure 4. Carbachol excites the SLDsp neurons through the activation of an Na^+–Ca^{2+} exchanger
A, carbachol (15 μM) activates an inward current across the entire voltage ramp, resulting in a parallel shift of the current–voltage relationship. *B*, blocking K^+ conductances with $BaCl_2$ (1 mM) does not block the effect of carbachol. *C–F*, the effect of carbachol is instead blocked by replacing 80% of extracellular Na^+ with choline chloride (low-Na^+ ACSF; *C*), is reduced by BAPTA (10 mM in the recording pipette; *D*) and is blocked by EGTA (10 mM in the recording pipette; *E*) or by the Na^+–Ca^{2+} exchanger blocker, KB-R7943 (KB-R; 35 μM; *F*). All the current–voltage relationships were obtained using voltage ramps (from −100 to −40 mV; 6 mV s^{-1}). *G*, examples of voltage-clamp recordings (V_h = −60 mV) before and during carbachol applications in $BaCl_2$ (1 mM), low-Na^+ ACSF, with BAPTA (10 mM) or EGTA (10 mM) in the recording pipette, and in KB-R7943. *H*, summary histogram of carbachol-mediated current recorded in control ACSF (con; $n = 22$; data also represented in Fig. 3*H*), in $BaCl_2$ ($BaCl_2$; $n = 6$), in low-Na^+ ACSF (low Na^+; $n = 8$), with BAPTA or EGTA in the recording pipette (BAPTA, $n = 8$; and EGTA, $n = 7$) and in KB-R7943 (KB-R; $n = 12$). $^{**}P < 0.01$, Student's paired *t* test, comparing holding currents before and during carbachol applications. ††$P < 0.01$, $F_{(5,57)} = 18.04$, $P < 0.001$, one-way ANOVA, Fisher's PLSD, comparing carbachol-mediated current in control ACSF (con) *vs.* the carbachol-mediated current of the pharmacologically treated groups ($BaCl_2$, low Na^+, BAPTA, EGTA and KB-R). All recordings were conducted in TTX (1 μM).

reduced it to 53.1 ± 15.0% (n = 7). Combined application of VU0255035 and J104129 (VU0255035 1 μM + J104129 50 nM) abolished carbachol-mediated current (−3.9 ± 1.6 pA; n = 5; P > 0.05, Student's paired t test, carbachol + VU0255035 + J104129 *vs.* VU0255035 + J104129). Altogether, these results strongly suggest that the carbachol-mediated excitation of the SLDsp neurons occurs by co-activation of M_1 and M_3 receptor subtypes (Fig. 3).

Carbachol excites SLDsp neurons through the activation of an Na^+–Ca^{2+} exchanger

We next examined the ionic mechanisms mediating carbachol excitation of SLDsp neurons. We first determined the current–voltage (I–V) relationship of the carbachol response using a voltage ramp protocol (from −100 to −40 mV, at 6 mV s^{-1}). We then tested whether cations that can block K^+ conductances could block the response of carbachol (Fig. 4). Barium chloride (1 mM) did not affect the carbachol-evoked inward current (−23.50 ± 3.42 pA; n = 6; P < 0.01, Student's paired t test, carbachol + $BaCl_2$ *vs.* $BaCl_2$; and P = 0.38, one-way ANOVA, carbachol in $BaCl_2$ *vs.* carbachol in control ACSF), indicating that the effect of carbachol was not mediated through a K^+ conductance. Carbachol produced an inward current across the entire voltage ramp, resulting in a parallel shift of the I–V relationship. This suggested that the reversal potential of the carbachol-mediated current is at a potential far from the range of potentials of our ramp protocol. It has been previously reported that carbachol excites basal forebrain neurons through activation of the Na^+–Ca^{2+} exchanger (Xu *et al.* 2006), which based on the composition of our extracellular and pipette solutions and a 3 Na^+:1 Ca^{2+} stoichiometry, has a predicted reversal potential of approximately +175 mV (Weber *et al.* 2002). To test whether the effect of carbachol was mediated through an Na^+–Ca^{2+} exchanger, we used the following three approaches: (i) we lowered the Na^+ gradient across the membrane; (iii) we buffered intracellular Ca^{2+}; and (iii) we blocked the Na^+–Ca^{2+} exchanger with KB-R7943. We first replaced 80% of extracellular Na^+ with choline chloride (low-Na^+ ACSF) and increased the concentration of Na^+ in the recording pipette to 10 mM. This shifted the predicted reversal potential of the Na^+–Ca^{2+} exchanger to approximately −55 mV and abolished carbachol-evoked inward current (−0.85 ± 0.57 pA; n = 8; P > 0.05, Student's paired t test, carbachol in low-Na^+ ACSF *vs.* control low-Na^+ ACSF). The carbachol response was also sensitive to intracellular free Ca^{2+}. We found that the response to carbachol was greatly reduced when we buffered intracellular Ca^{2+} with 1,2-bis-(o-aminophen-oxy)ethane-N,N,N′,N′-tetraacetic acid (BAPTA; 10 mM in the recording pipette; −7.53 ± 1.43 pA; n = 8; P < 0.01, Student's paired t test, carbachol with BAPTA *vs.* control conditions with BAPTA) and it was blocked by EGTA (10 mM in the recording pipette; −2.20 ± 1.38 pA; n = 7; P > 0.05, Student's paired t test, carbachol with EGTA *vs.* control conditions with EGTA). In addition, application of KB-R7943 (35 μM), which at this concentration inhibits the Na^+–Ca^{2+} exchanger in forward mode (Iwamoto *et al.* 1996), completely blocked the carbachol-mediated inward current (−0.79 ± 1.75 pA; n = 12; P > 0.05, Student's paired t test, carbachol + KB-R7943 *vs.* KB-R7943). Altogether, these results strongly suggest that carbachol directly excites SLDsp neurons by activating an Na^+–Ca^{2+} exchanger (Fig. 4).

Carbachol increases glutamatergic input to SLDsp neurons through presynaptic M_1 and M_3 muscarinic receptors

We next examined the effects of carbachol on glutamatergic input to SLDsp neurons. Carbachol (15 μM) administration nearly doubled the frequency of glutamatergic sEPSCs (control conditions, 3.15 ± 1.00 Hz and carbachol, 6.12 ± 1.32 Hz; n = 8; P < 0.01, Student's paired t test; Fig. 5). This effect was reversed after 20 min if washout, and the sEPSCs were completely abolished by the AMPA receptor antagonist DNQX (20 μM; n = 3; recordings in 10 μM bicuculline at V_h = −60 mV).

To determine whether carbachol acts on presynaptic glutamatergic terminals, we tested its effects on glutamatergic mEPSCs. Carbachol increased the frequency of glutamatergic mEPSCs by 66% (control conditions, 1.12 ± 0.18 Hz and carbachol, 1.87 ± 0.37 Hz; n = 10; P < 0.01, Student's paired t test; and washout, 1.07 ± 0.21 Hz). Carbachol had no effect on mEPSC amplitude (control conditions, 12.65 ± 1.13 pA and carbachol, 12.44 ± 1.17 pA; n = 10; P = 0.59, Student's paired t test; washout, 11.97 ± 1.36 pA), consistent with a presynaptic effect. Application of scopolamine (10 μM) completely blocked the effects of carbachol on mEPSC frequency (scopolamine, 0.80 ± 0.14 Hz and scopolamine + carbachol, 0.78 ± 0.14 Hz; n = 8; P = 0.83, Student's paired t test), indicating that carbachol acts presynaptically through muscarinic receptors (Fig. 5).

Application of pirenzepine (preferential M_1 receptor antagonist) or 4-DAMP (preferential M_3/M_1 receptor antagonist) reduced but did not block the effect of carbachol on mEPSC frequency (Fig. 6). In the presence of pirenzepine (10 μM), carbachol still increased the frequency of glutamatergic mEPSCs by 44% (pirenzepine, 1.21 ± 0.12 Hz and pirenzepine + carbachol, 1.74 ± 0.15 Hz; n = 8; P = 0.007, Student's paired t test), whereas in 4-DAMP (100 nM), carbachol increased

mEPSC frequency by only 14% (4-DAMP, 0.74 ± 0.07 Hz and 4-DAMP + carbachol, 0.85 ± 0.09 Hz; $n = 10$; $P = 0.013$, Student's paired t test). Combined application of pirenzepine and 4-DAMP (10 μM pirenzepine + 100 nM 4-DAMP) completely abolished the effects of carbachol on the mEPSC frequency (pirenzepine + 4-DAMP, 1.70 ± 0.21 Hz and pirenzepine + 4-DAMP + carbachol, 1.69 ± 0.25 Hz; $n = 6$; $P = 0.95$, Student's paired t test), whereas combined application of the preferential M_2/M_4 receptor antagonist AQ-RA-741 and the M_4-selective receptor antagonist PD102807 (200 nM AQ-RA-741 + 1 μM PD102807) was ineffective (AQ-RA-741 + PD102807, 1.26 ± 0.19 Hz and AQ-RA-741 + PD102807 + carbachol, 2.23 ± 0.29 Hz, $n = 7$; $P = 0.026$, Student's paired t test). This suggests that carbachol increases the glutamatergic input to the SLDsp neurons through M_1 and/or M_3, but not through M_2 and M_4 presynaptic receptors (Fig. 6).

To test this possibility further, we used VU0255035 (M_1-selective antagonist; Sheffler *et al.* 2009) and J104129 (M_3-selective antagonist; Mitsuya *et al.* 1999). Both these antagonists reduced the effect of carbachol on mEPSC

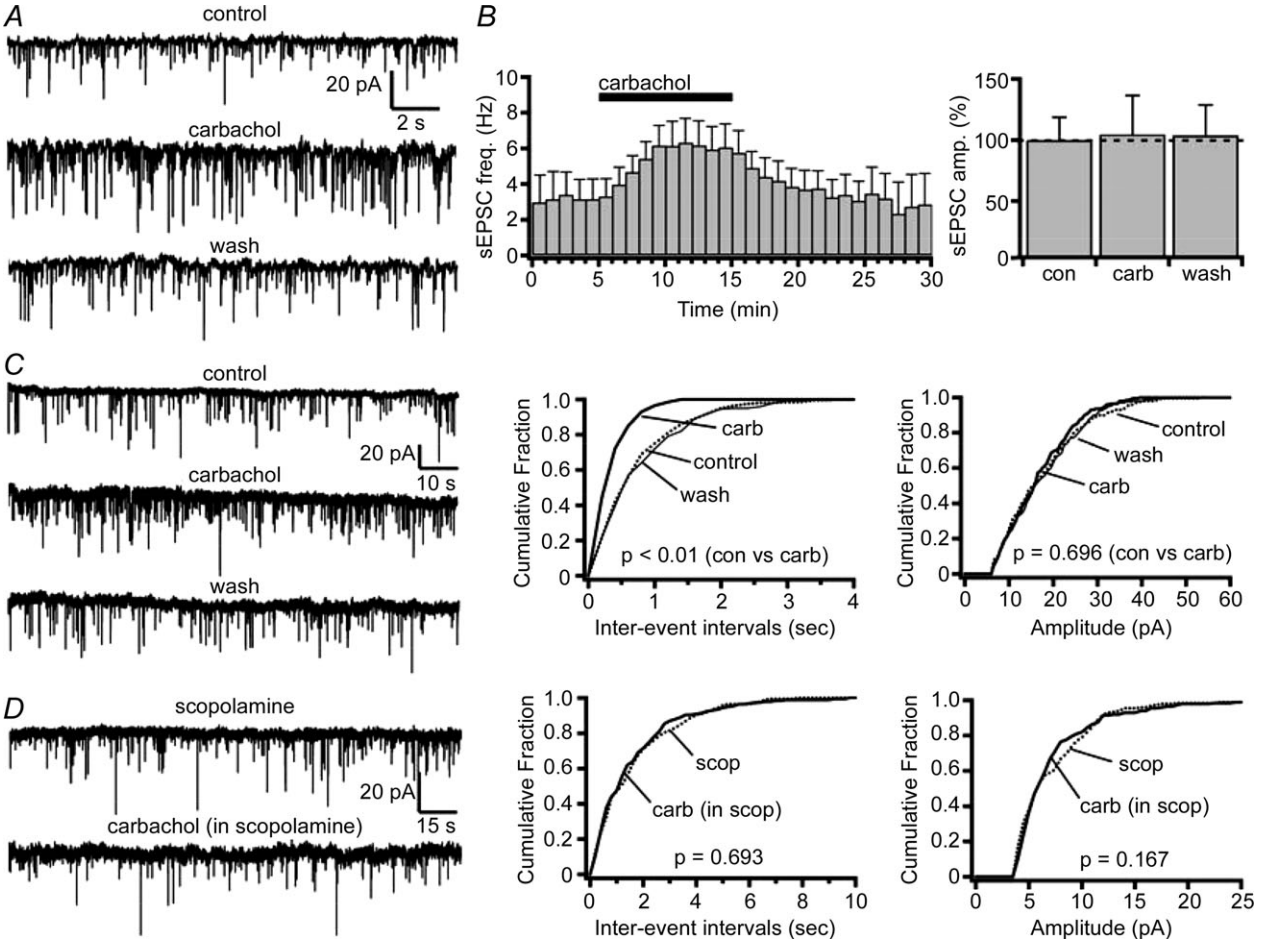

Figure 5. The presynaptic effect of carbachol
A, carbachol (15 μM) increases spontaneous excitatory postsynaptic current (sEPSC) frequency without affecting amplitude. Current traces are shown for a representative SLDsp neuron in control, carbachol and washout (wash) conditions. *B*, mean effect of carbachol on sEPSC frequency ($n = 8$; left panel) and sEPSC amplitude ($F_{(2,19)} = 0.641$, $P = 0.547$, one-way ANOVA; right panel). *C*, effects of carbachol on the miniature excitatory postsynaptic currents (mEPSCs) shown in a representative SLDsp neuron. The current traces are represented in the left panel and the cumulative distribution plots of mEPSC interevent interval and amplitude are represented in the centre and right panels, respectively. Carbachol significantly decreases the interevent interval without affecting the mEPSC amplitude (P values from Kolmogorov–Smirnov test). *D*, the effect of carbachol is completely abolished in the presence of scopolamine (10 μM), indicating that carbachol acts on presynaptic muscarinic receptors (current traces for scopolamine and scopolamine + carbachol are represented in the left panel; cumulative distribution plots of the mEPSC interevent interval and amplitude are represented in the centre and right panels, respectively; P values from Kolmogorov–Smirnov test). Spontaneous EPSCs and mEPSCs were recorded at $V_h = -60$ mV, and mEPSCs were recorded in TTX (1 μM). In the cumulative distributions, results are represented before carbachol application as dotted lines, during carbachol as bold lines and after carbachol application as thinner lines.

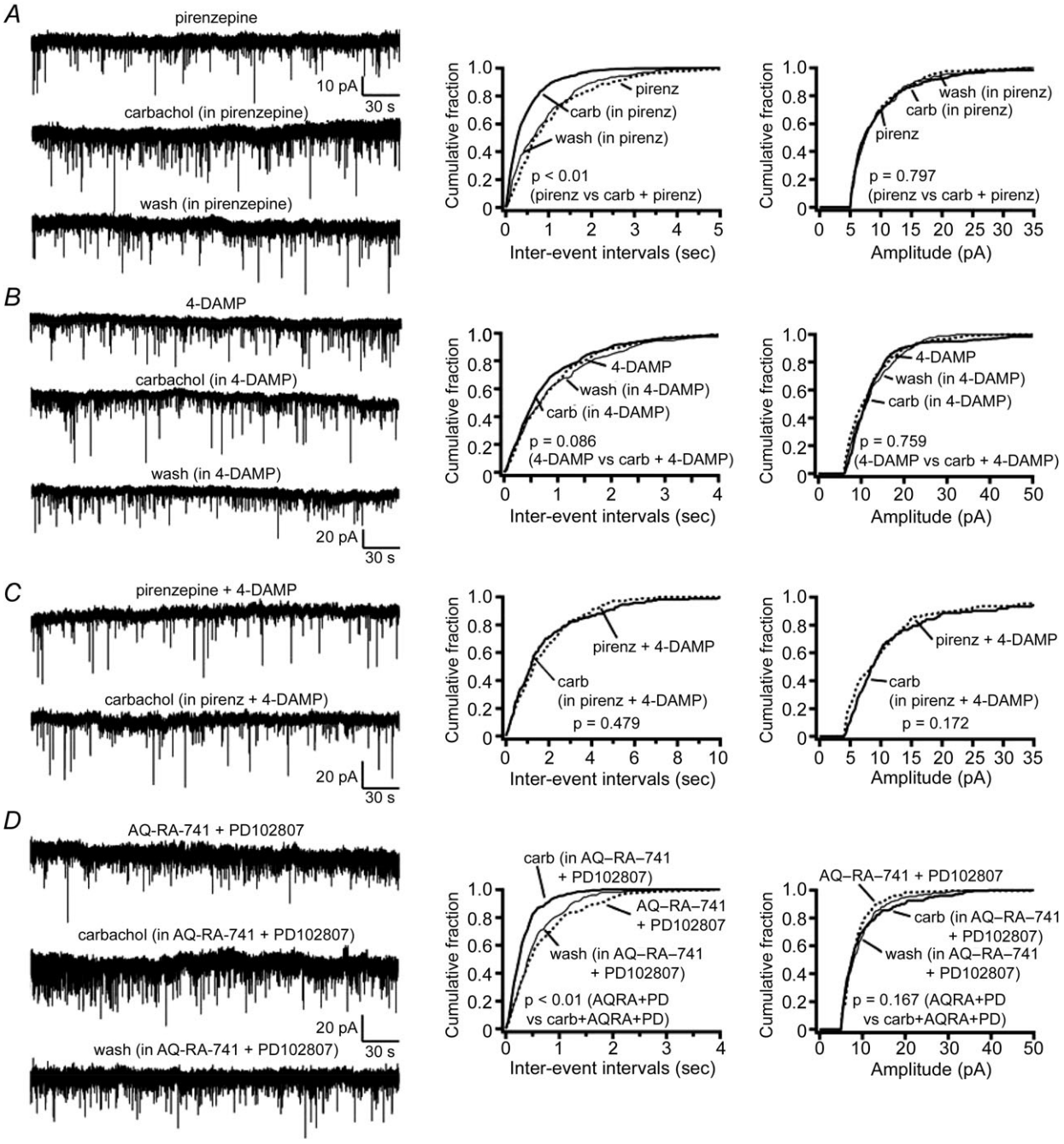

Figure 6. The presynaptic effect of carbachol is mediated by M_1/M_3 but not M_2/M_4 muscarinic receptors
A and *B*, the preferential M_1 receptor antagonist pirenzepine (10 μM; *A*) or the preferential M_3/M_1 receptor antagonist 4-DAMP (100 nM; *B*) lead to only a partial block of the effects of carbachol on the mEPSC frequency. *C*, co-application of pirenzepine + 4-DAMP abolishes the effects of carbachol. *D*, co-application of the preferential M_2/M_4 receptor antagonist AQ-RA-741 (200 nM) and the M_4-selective receptor antagonist PD102807 (1 μM) are ineffective in reversing the effects of carbachol on mEPSC frequency. Effects of carbachol on the mEPSCs in the presence of pirenzepine, 4-DAMP, pirenzepine + 4-DAMP and AQ-RA-741 + PD102807 are shown in four representative SLDsp neurons. The current traces are represented in the left panels and the cumulative distribution plots of mEPSC interevent interval and amplitude are represented in the centre and right panels, respectively. Miniature EPSCs were recorded in TTX (1 μM) at $V_h = -60$ mV. In the cumulative distributions, results are represented before carbachol application as dotted lines, during carbachol as bold lines and after carbachol application as thinner lines, and *P* values refer to Kolmogorov–Smirnov tests.

frequency but did not abolish it (Fig. 7). In the presence of VU0255035 (1 μM), carbachol increased the mEPSC frequency by 46% (VU0255035, 1.13 ± 0.08 Hz and VU0255035 + carbachol, 1.64 ± 0.16 Hz; $n = 7$; $P = 0.007$, Student's paired t test), whereas in J104129 (50 nM), carbachol increased the glutamatergic mEPSC frequency by 25% (J104129, 1.31 ± 0.16 Hz and J104129 + carbachol, 1.64 ± 0.24 Hz; $n = 7$; $P = 0.024$, Student's paired t test). Combined application of VU0255035 and J104129 (1 μM VU0255035 + 50 nM J104129) completely abolished the effects of carbachol on the mEPSC frequency (VU0255035 + J104129, 1.63 ± 0.34 Hz and VU0255035 + J104129 + carbachol, 1.56 ± 0.37 Hz; $n = 5$; $P = 0.58$, Student's paired t test). These results indicate that carbachol increases the glutamatergic input to the SLDsp neurons through both M_1 and M_3 presynaptic receptors, with the predominant effect occurring through the M_3 subtype.

Discussion

We found that carbachol excites SLDsp neurons both through a direct postsynaptic effect and by increasing glutamatergic synaptic inputs. Both of these effects were mediated through M_1 and M_3 receptors and strongly suggest cellular mechanisms through which acetylcholine can contribute to the generation of atonia during REM sleep.

Carbachol directly excites the SLDsp neurons through M_1 and M_3 muscarinic receptors

Previous *in vivo* single-unit recording studies in cats reported that iontophoretic application of carbachol activates REM sleep-active neurons in the SLD (Sakai *et al.* 2001). Identifying and studying these neurons *in vitro* has been a challenge because the SLD contains a great variety of cell types, including glutamatergic, noradrenergic and GABAergic neurons (Lu *et al.* 2006; VanderHorst & Ulfhake, 2006; Brown *et al.* 2008; Bruinstroop *et al.* 2011) and lacks markers specific for REM sleep-active neurons. It is therefore not surprising that previous *in vitro* studies have found both excitatory and inhibitory responses to carbachol in neurons of the SLD region in rats and mice (Brown *et al.* 2006; Garcia-Rill *et al.* 2007; Heister *et al.* 2009). Our findings, which derive from a selective interrogation of spinally projecting SLD neurons, reveal that carbachol directly and consistently excites SLDsp neurons through postsynaptic muscarinic receptors.

Of the five known muscarinic receptor subtypes, the M_1, M_2 and M_3 subtypes are expressed in the SLD region (Baghdoyan *et al.* 1994; Mallios *et al.* 1995). We selected a combination of widely used antagonists that have poor receptor subtype specificity, namely pirenzepine (M_1 preferring), 4-DAMP (M_3/M_1 preferring) and AQ-RA-741 (M_2/M_4 preferring), as well as three recently developed subtype-selective antagonists, namely VU0255035 (M_1 selective; Sheffler *et al.* 2009), J104129 (M_3 selective; Mitsuya *et al.* 1999) and PD102807 (M_4 selective; Kitaichi *et al.* 1999). We found that the effect of carbachol on SLDsp neurons was mediated by the M_1 and M_3 receptor subtypes, but not M_2 and M_4. The M_2 receptor is thought to be the predominant subtype expressed in GABAergic neurons of the pontine reticular formation, but not in glutamatergic SLDsp neurons (Coleman *et al.* 2004; Brischoux *et al.* 2008). Our results are generally consistent with this finding. The M_1 subtype activates SLD neurons *in vitro* (Heister *et al.* 2009), but it has been reported that manipulation of the M_1 receptors in the SLD failed to produce effects on REM sleep (Velazquez-Moctezuma *et al.* 1991; Coleman *et al.* 2004). It was therefore surprising to find in the present study that M_1 receptors contribute to the carbachol-mediated excitation of SLDsp neurons. In contrast, and in agreement with our findings, the M_3 subtype is thought to activate the pontine REM generator neurons directly (Sakai & Onoe 1997).

In conclusion, our combined electrophysiological and pharmacological approach demonstrates that SLDsp neurons are excited by carbachol and that this response is mediated by the combined activation of M_3 as well as M_1 postsyanaptic receptors.

Our experiments also revealed that the postsynaptic effect of carbachol on SLDsp neurons is mediated by activation of an Na^+–Ca^{2+} exchanger. This conclusion is supported by the sensitivity of the carbachol-mediated inward current to extracellular Na^+ and intracellular Ca^{2+} concentrations, as well as to KB-R7943, a selective inhibitor of the Na^+–Ca^{2+} exchanger. The Na^+–Ca^{2+} exchangers are Ca^{2+} transporters that extrude Ca^{2+} from the cytoplasm with an exchange ratio of three Na^+ ions brought in for every extruded Ca^{2+} ion (i.e. forward mode). This activity generates a net influx of positive charges that results in a steady-state inward current and can be accompanied by an increase in membrane current noise (Xu *et al.* 2006). All three isoforms of the Na^+–Ca^{2+} exchangers (NCX1, NCX2 and NCX3) are expressed in the brain (Lytton, 2007). In addition to acetylcholine, other neurotransmitters, such as orexin-A and thyrotrophin-releasing hormone, excite target neurons through Gq-coupled signalling and activation of Na^+–Ca^{2+} exchangers (Eriksson *et al.* 2001; Burdakov *et al.* 2003; Xu *et al.* 2006; Parmentier *et al.* 2009). A debate continues, however, over whether these neurotransmitters directly affect the Na^+–Ca^{2+} exchangers or, rather, that their increased activity is a consequence of increased intracellular Ca^{2+} levels. In addition, a

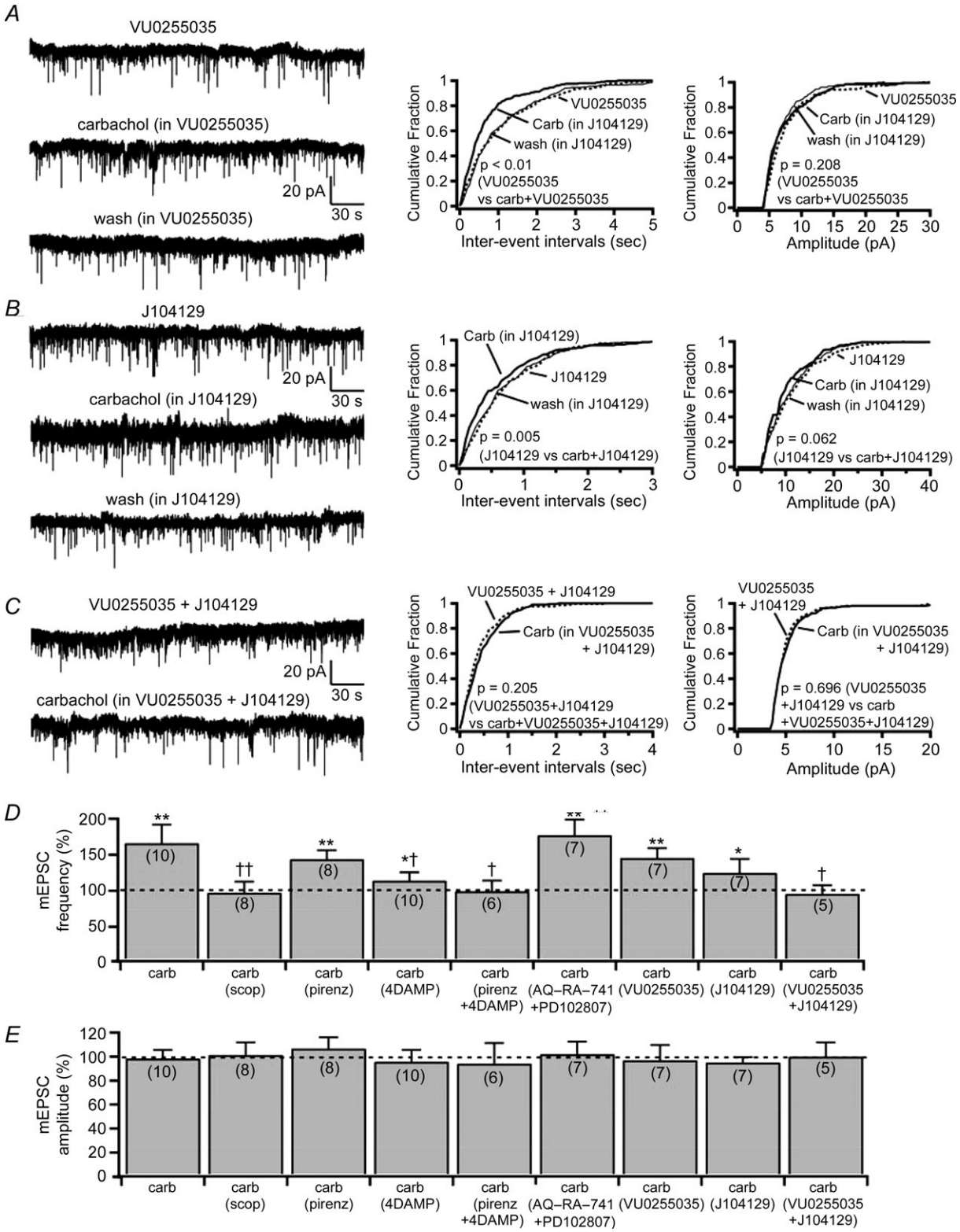

Figure 7. Carbachol increases glutamatergic input to SLDsp neurons by co-activation of presynaptic M_1 and M_3 muscarinic receptors

A and *B*, the M_1-selective and the M_3-selective muscarinic receptor antagonists, VU0255035 (1 μM) and J104129 (50 nM), produce only a partial block of the effects of carbachol on the mEPSC frequency. *C*, co-application VU0255035 (1 μM) + J104129 (50 nM) abolishes the effects of carbachol. The effects of carbachol on the mEPSCs in the presence of VU0255035, J104129 and VU0255035 + J104129 are shown in three representative SLDsp

carbachol-mediated increase in intracellular Ca^{2+} levels could also produce an increase in the voltage-gated Na^+ currents (Bulatko & Greeff, 1995). Still, the lack of changes in the action potential amplitude, duration and threshold in response to carbachol suggests that it is unlikely that modulation of the voltage-gated Na^+ current contributes to the carbachol-mediated excitation of SLDsp neurons. In further support of a mechanism for the activation of the Na^+–Ca^{2+} exchanger through intracellular Ca^{2+} elevation are the observations that Gq signalling pathways can activate intracellular Ca^{2+} signalling and that Na^+–Ca^{2+} exchangers become maximally activated when Ca^{2+} rises above resting levels (Lytton, 2007). Future studies using Ca^{2+} imaging might be able to provide a definitive answer concerning this mechanism of action. Nevertheless, it is clear that, directly or indirectly, the activation of the Na^+–Ca^{2+} exchangers depolarizes the membrane potential and promotes neuronal Firing.

Carbachol acts through presynaptic M_1 and M_3 muscarinic receptors to increase excitatory inputs to SLDsp neurons

Previous microdialysis studies have suggested that glutamatergic input to SLD neurons is important in REM sleep regulation. Injection of glutamate receptor agonists into the SLD region of cats and rats increased the firing of SLD REM-active neurons and induced a REM-like state with continuous muscle atonia (Lai & Siegel, 1991; Onoe & Sakai, 1995; Hajnik *et al.* 2000). Kynurenate, a glutamate antagonist, rapidly reversed the muscle atonia induced by local application of bicuculline in rats, but did not alter the cortical REM-like state, suggesting that the glutamatergic input to the SLD is required for the generation of atonia during REM sleep (Boissard *et al.* 2002). We found that carbachol increases glutamatergic synaptic drive to SLDsp neurons, which may serve as an additional excitatory mechanism for cholinergic activation of atonia pathways. This observation runs counter to a previous electrophysiological *in vitro* study, which found that carbachol mostly reduced the glutamatergic input to neurons in the SLD region of rats (Heister *et al.* 2009). However, that study did not identify the phenotype of the recorded neurons, and it is not clear to what extent the recordings included SLDsp neurons. We also found that carbachol increased the frequency of mEPSCs without affecting their amplitude, indicating a presynaptic effect with no change in postsynaptic efficacy. Using the same pharmacological approach that we used to identify the muscarinic receptor subtypes responsible for the postsynaptic response to carbachol, we found that the effect of carbachol on the mEPSC frequency was abolished by scopolamine (non-subtype selective) or by co-application of an M_1- and an M_3-selective antagonist, namely VU0255035 (M_1 selective; Sheffler *et al.* 2009) and J104129 (M_3 selective; Mitsuya *et al.* 1999), which is consistent with a muscarinic presynaptic response mediated by M_1 and M_3 receptor subtypes. Our pharmacological study also shows that the M_3 receptors are the larger contributor of the presynaptic response to carbachol.

Methods to detect glutamatergic neurons definitively by the presence of vesicular transporters are relatively new. Previous studies on glutamatergic inputs to the SLD used glutamate antibodies, which are neither sensitive nor specific. Hence, the source of glutamatergic input to the SLD remains unknown. The lateral hypothalamus, ventrolateral periaqueductal grey matter, lateral pontine tegmentum and ventrolateral medulla all contain glutamatergic neurons and project to the SLD (Shammah-Lagnado *et al.* 1987; Lai *et al.* 1993; Semba, 1993; Boissard *et al.* 2003), although it is not known whether the neurons projecting to the SLD from these regions are glutamatergic. A small number of cells in the contralateral SLD region and a larger number of cells in the

neurons. The current traces are represented in the left panels and the cumulative distribution plots of mEPSC interevent interval and amplitude are represented in the centre and right panels, respectively. *D* and *E*, summary bar graphs compare the effects on mEPSC frequency (*D*) and mEPSC amplitude (*E*) of carbachol applied alone ($n = 10$) and in the presence of scopolamine (10 μM, $n = 8$), pirenzepine (10 μM, $n = 8$), 4-DAMP (100 nM, $n = 10$), 4-DAMP + pirezepine ($n = 6$), AQ-RA-741 (200 nM) + PD102807 (1 μM, $n = 7$), VU0255035 (1 μM, $n = 7$), J104129 (50 nM, $n = 7$), and VU0255035 + J104129 ($n = 5$). $^*P < 0.05$ and $^{**}P < 0.01$, Student's paired *t* test comparing the effects on mEPSC frequency and mEPSC amplitude before and during carbachol applications (carb *vs.* con; scop + carb *vs.* scop; pirenz + carb *vs.* pirenz; 4-DAMP + carb *vs.* 4-DAMP; pirenz + 4-DAMP + carb *vs.* pirenz + 4-DAMP; AQ-RA-741 + PD102807 + carb *vs.* AQ-RA-741 + PD102807; VU0255035 + carb *vs.* VU0255035; J104129 + carb *vs.* J104129; and VU0255035 + J104129 + carb *vs.* VU0255035 + J104129). Effects of carbachol on mEPSC frequency ($F_{(8,59)} = 2.635$, $P = 0.015$, one-way ANOVA) and mEPSC amplitude ($F_{(8,59)} = 0.153$, $P = 0.996$, one-way ANOVA), †$P < 0.05$ and ††$P < 0.01$, Fisher's PLSD comparing the effects of carbachol in control ACSF and in the presence of muscarinic receptor antagonists (carb *vs.* carb in scop; carb *vs.* carb in pirenz; carb *vs.* carb in 4-DAMP; carb *vs.* carb in pirenz + 4-DAMP; carb *vs.* carb in AQ-RA-741 + PD102807; carb *vs.* carb in VU0255035; carb *vs.* carb in J104129; and carb *vs.* carb + VU0255035 + J104129). Miniature EPSCs were recorded in TTX (1 μM) at $V_h = -60$ mV. In the cumulative distributions, results are represented before carbachol application as dotted lines, during carbachol application as bold lines and after carbachol application as thinner lines, and *P* values refer to Kolmogorov–Smirnov tests.

ipsi- and contralateral pontine reticular formation were found to project to the SLD (Lai *et al.* 1993; Boissard *et al.* 2003), but their phenotype, too, remains unidentified. In addition, it is still unclear whether glutamatergic input to the SLD REM-atonia neurons is stable across all behavioural states or whether it increases at the onset of REM sleep. Our results suggest that a muscarinic presynaptic mechanism increases glutamatergic input to SLD neurons during REM sleep when the levels of acetylcholine in the dorsal pons are highest (Leonard & Lydic, 1997). Defining which of these glutamatergic inputs contribute to the development of atonia should be achievable using optogenetic stimulation or other techniques.

Physiological significance and neuronal circuitry controlling REM muscle atonia

Based on present and prior results, it appears most likely that acetylcholine promotes REM sleep in the dorsomedial pons by activating two separate sets of REM-generating neurons; the first set promotes cortical activation through ascending inputs to the thalamus, the posterior hypothalamus and the basal forebrain, whereas the second set generates muscle atonia through descending inputs to glycinergic/GABAergic premotor neurons in the spinal cord and ventral medulla (Fuller *et al.* 2007; Luppi *et al.* 2012; Chase, 2013). The existence of separate pathways mediating the cortical and motor components of REM sleep also provides a possible basis for the occasional dissociation of atonia and cortical activation during pathological states such as cataplexy, sleep paralysis and REM sleep behaviour disorder (Lu *et al.* 2006; Vetrivelan *et al.* 2009, 2011; Luppi *et al.* 2011). There is general consensus that descending projections for REM atonia originate from glutamatergic REM sleep-active neurons of the SLD, and that during REM sleep the motorneurons are actively inhibited by glycinergic and GABAergic inputs and through ionotrophic glycine and $GABA_A$ receptors and metabotropic $GABA_B$ receptors (Chase *et al.* 1989; Brooks & Peever, 2012; Chase, 2013). There remains, however, an open debate over the respective contribution of premotor neurons of the ventromedial medulla *vs.* spinal interneurons in mediating REM atonia (Chase, 2013). Moreover, it is possible that premotor neurons in the medulla and spinal ventral horn are activated by distinct groups of SLD neurons. Along these lines, a previous single-unit recording study in cats found that spinally projecting neurons in the peri-LCα were inactive during REM sleep (Sakai *et al.* 1981). Importantly, however, only a relatively small number of neurons were sampled, and many of these may have been noradrenergic neurons, which are known to be silent during REM sleep (Aston-Jones & Bloom, 1981; Bruinstroop *et al.* 2011). Indeed, in cats, glutamatergic subcoeruleus neurons are intermingled with noradrenergic neurons of the LC complex. Therefore, while the medullary pathway may contribute to atonia in intact animals, the available data continue to suggest that the SLD–spinal cord pathway is necessary to produce muscle atonia during REM sleep; hence, it was the focus of the present study.

Although the amount and onset of REM sleep generated by local administration of carbachol to the pons vary depending on the location and dose of the injections, species or type of preparation (Kubin, 2001), the classical hypothesis that cholinergic neurons participate in the genesis of REM sleep is still widely accepted. Indeed, acetylcholine levels in the dorsal pons are twice as high in REM sleep compared with slow-wave sleep and wakefulness (Leonard & Lydic, 1997), and depletion of acetylcholine inhibits REM sleep, whereas blocking acetylcholine degradation promotes REM sleep (reviewed by Jones, 1991). These findings are also consistent with the report of innervation of the SLD by choline acetyltransferase-immunoreactive fibres that originate in the pedunculuopontine and laterodorsal tegmental nuclei (Jones, 1990; Semba, 1993). Our results provide important insights into the cellular mechanisms by which acetylcholine can activate SLD REM-atonia neurons.

Our findings indicate that acetylcholine produces synergistic, excitatory pre- and postsynaptic effects on spinally projecting SLD neurons. These effects should promote muscle atonia during REM sleep. Simultaneous withdrawal of monoaminergic, orexinergic and GABAergic neurotransmission onto SLD neurons may also contribute to muscle atonia (Jones, 1991; Vetrivelan *et al.* 2011; Luppi *et al.* 2012); however, how these neurotransmitters and peptides affect the SLD REM-atonia neurons is still poorly understood and is of considerable interest for future studies.

References

Aston-Jones G & Bloom FE (1981). Activity of norepinephrine-containing locus coeruleus neurons in behaving rats anticipates fluctuations in the sleep-waking cycle. *J Neurosci* **1**, 876–886.

Baghdoyan HA (1997). Cholinergic mechanisms regulating REM sleep. In *Sleep Science: IntegratingBasic Research and Clinical practice*, ed. Schwartz W.J., pp. 88–116. Karger Publishing, Basel.

Baghdoyan HA, Mallios VJ, Duckrow RB & Mash DC (1994). Localization of muscarinic receptor subtypes in brain stem areas regulating sleep. *Neuroreport* **5**, 1631–1634.

Boeve BF, Silber MH, Saper CB, Ferman TJ, Dickson DW, Parisi JE, Benarroch EE, Ahlskog JE, Smith GE, Caselli RC, Tippman-Peikert M, Olson EJ, Lin SC, Young T, Wszolek Z, Schenck CH, Mahowald MW, Castillo PR, Del Tredici K & Braak H (2007). Pathophysiology of REM sleep behaviour disorder and relevance to neurodegenerative disease. *Brain* **130**, 2770–2788.

Boissard R, Fort P, Gervasoni D, Barbagli B & Luppi PH (2003). Localization of the GABAergic and non-GABAergic neurons projecting to the sublaterodorsal nucleus and potentially gating paradoxical sleep onset. *Eur J Neurosci* **18**, 1627–1639.

Boissard R, Gervasoni D, Schmidt MH, Barbagli B, Fort P & Luppi PH (2002). The rat ponto-medullary network responsible for paradoxical sleep onset and maintenance: a combined microinjection and functional neuroanatomical study. *Eur J Neurosci* **16**, 1959–1973.

Brischoux F, Mainville L & Jones BE (2008). Muscarinic-2 and orexin-2 receptors on GABAergic and other neurons in the rat mesopontine tegmentum and their potential role in sleep–wake state control. *J Comp Neurol* **510**, 607–630.

Brooks PL & Peever JH (2012). Identification of the transmitter and receptor mechanisms responsible for REM sleep paralysis. *J Neurosci* **32**, 9785–9795.

Brown RE, McKenna JT, Winston S, Basheer R, Yanagawa Y, Thakkar MM & McCarley RW (2008). Characterization of GABAergic neurons in rapid-eye-movement sleep controlling regions of the brainstem reticular formation in GAD67-green fluorescent protein knock-in mice. *Eur J Neurosci* **27**, 352–363.

Brown RE, Winston S, Basheer R, Thakkar MM & McCarley RW (2006). Electrophysiological characterization of neurons in the dorsolateral pontine rapid-eye-movement sleep induction zone of the rat: intrinsic membrane properties and responses to carbachol and orexins. *Neuroscience* **143**, 739–755.

Bruinstroop E, Cano G, Vanderhorst VG, Cavalcante JC, Wirth J, Sena-Esteves M & Saper CB (2011). Spinal projections of the A5, A6 (locus coeruleus), and A7 noradrenergic cell groups in rats. *J Comp Neurol* **520**, 1985–2001.

Buckley NJ, Bonner TI, Buckley CM & Brann MR (1989). Antagonist binding properties of five cloned muscarinic receptors expressed in CHO-K1 cells. *Mol Pharmacol* **35**, 469–476.

Bulatko AK & Greeff NG (1995). Functional availability of sodium channels modulated by cytosolic free Ca^{2+} in cultured mammalian neurons (N1E-115). *J Physiol* **484**, 307–312.

Burdakov D, Liss B & Ashcroft FM (2003). Orexin excites GABAergic neurons of the arcuate nucleus by activating the sodium–calcium exchanger. *J Neurosci* **23**, 4951–4957.

Chase MH (2013). Motor control during sleep and wakefulness: clarifying controversies and resolving paradoxes. *Sleep Med Rev* **17**, 299–312.

Chase MH, Soja PJ & Morales FR (1989). Evidence that glycine mediates the postsynaptic potentials that inhibit lumbar motoneurons during the atonia of active sleep. *J Neurosci* **9**, 743–751.

Clement O, Sapin E, Berod A, Fort P & Luppi PH (2011). Evidence that neurons of the sublaterodorsal tegmental nucleus triggering paradoxical (REM) sleep are glutamatergic. *Sleep* **34**, 419–423.

Coleman CG, Lydic R & Baghdoyan HA (2004). M2 muscarinic receptors in pontine reticular formation of C57BL/6J mouse contribute to rapid eye movement sleep generation. *Neuroscience* **126**, 821–830.

Eriksson KS, Sergeeva O, Brown RE & Haas HL (2001). Orexin/hypocretin excites the histaminergic neurons of the tuberomammillary nucleus. *J Neurosci* **21**, 9273–9279.

Franklin FBJ & Paxinos G (1997). *The Mouse Brain in Stereotaxic Coordinates*. Academic Press Inc., San Diego, CA, USA.

Fuller PM, Saper CB & Lu J (2007). The pontine REM switch: past and present. *J Physiol* **584**, 735–741.

Gagnon JF, Postuma RB, Mazza S, Doyon J & Montplaisir J (2006). Rapid-eye-movement sleep behaviour disorder and neurodegenerative diseases. *Lancet Neurol* **5**, 424–432.

Garcia-Rill E, Heister DS, Ye M, Charlesworth A & Hayar A (2007). Electrical coupling: novel mechanism for sleep-wake control. *Sleep* **30**, 1405–1414.

Hajnik T, Lai YY & Siegel JM (2000). Atonia-related regions in the rodent pons and medulla. *J Neurophysiol* **84**, 1942–1948.

Heister DS, Hayar A & Garcia-Rill E (2009). Cholinergic modulation of GABAergic and glutamatergic transmission in the dorsal subcoeruleus: mechanisms for REM sleep control. *Sleep* **32**, 1135–1147.

Iwamoto T, Watano T & Shigekawa M (1996). A novel isothiourea derivative selectively inhibits the reverse mode of Na^+/Ca^{2+} exchange in cells expressing NCX1. *J Biol Chem* **271**, 22391–22397.

Jones BE (1990). Immunohistochemical study of choline acetyltransferase-immunoreactive processes and cells innervating the pontomedullary reticular formation in the rat. *J Comp Neurol* **295**, 485–514.

Jones BE (1991). Paradoxical sleep and its chemical/structural substrates in the brain. *Neuroscience* **40**, 637–656.

Kitaichi K, Day JC & Quirion R (1999). A novel muscarinic M_4 receptor antagonist provides further evidence of an autoreceptor role for the muscarinic M_2 receptor sub-type. *Eur J Pharmacol* **383**, 53–56.

Krenzer M, Anaclet C, Vetrivelan R, Wang N, Vong L, Lowell BB, Fuller PM & Lu J (2011). Brainstem and spinal cord circuitry regulating REM sleep and muscle atonia. *PLoS One* **6**, e24998.

Kubin L (2001). Carbachol models of REM sleep: recent developments and new directions. *Arch Ital Biol* **139**, 147–168.

Lai YY, Clements JR & Siegel JM (1993). Glutamatergic and cholinergic projections to the pontine inhibitory area identified with horseradish peroxidase retrograde transport and immunohistochemistry. *J Comp Neurol* **336**, 321–330.

Lai YY, Kodama T, Schenkel E & Siegel JM (2010). Behavioral response and transmitter release during atonia elicited by medial medullary stimulation. *J Neurophysiol* **104**, 2024–2033.

Lai YY & Siegel JM (1991). Pontomedullary glutamate receptors mediating locomotion and muscle tone suppression. *J Neurosci* **11**, 2931–2937.

Leonard TO & Lydic R (1997). Pontine nitric oxide modulates acetylcholine release, rapid eye movement sleep generation, and respiratory rate. *J Neurosci* **17**, 774–785.

Lu J, Sherman D, Devor M & Saper CB (2006). A putative flip-flop switch for control of REM sleep. *Nature* **441**, 589–594.

Luppi PH, Clement O, Sapin E, Gervasoni D, Peyron C, Leger L, Salvert D & Fort P (2011). The neuronal network responsible for paradoxical sleep and its dysfunctions causing narcolepsy and rapid eye movement (REM) behaviour disorder. *Sleep Med Rev* **15**, 153–163.

Luppi PH, Clement O, Sapin E, Peyron C, Gervasoni D, Leger L & Fort P (2012). Brainstem mechanisms of paradoxical (REM) sleep generation. *Pflugers Arch* **463**, 43–52.

Lytton J (2007). Na^+/Ca^{2+} exchangers: three mammalian gene families control Ca^{2+} transport. *Biochem J* **406**, 365–382.
McCarley RW (2007). Neurobiology of REM and NREM sleep. *Sleep Med* **8**, 302–330.
Mallios VJ, Lydic R & Baghdoyan HA (1995). Muscarinic receptor subtypes are differentially distributed across brain stem respiratory nuclei. *Am J Physiol Lung Cell Mol Physiol* **268**, L941–L949.
Mathis J, Hess CW & Bassetti C (2007). Isolated mediotegmental lesion causing narcolepsy and rapid eye movement sleep behaviour disorder: a case evidencing a common pathway in narcolepsy and rapid eye movement sleep behaviour disorder. *J Neurol Neurosurg Psychiatry* **78**, 427–429.
Mitsuya M, Mase T, Tsuchiya Y, Kawakami K, Hattori H, Kobayashi K, Ogino Y, Fujikawa T, Satoh A, Kimura T, Noguchi K, Ohtake N & Tomimoto K (1999). J-104129, a novel muscarinic M_3 receptor antagonist with high selectivity for M_3 over M_2 receptors. *Bioorg Med Chem* **7**, 2555–2567.
Morrison AR (1988). Paradoxical sleep without atonia. *Arch Ital Biol* **126**, 275–289.
Onoe H & Sakai K (1995). Kainate receptors: a novel mechanism in paradoxical (REM) sleep generation. *Neuroreport* **6**, 353–356.
Parmentier R, Kolbaev S, Klyuch BP, Vandael D, Lin JS, Selbach O, Haas HL & Sergeeva OA (2009). Excitation of histaminergic tuberomamillary neurons by thyrotropin-releasing hormone. *J Neurosci* **29**, 4471–4483.
Sakai K, Crochet S & Onoe H (2001). Pontine structures and mechanisms involved in the generation of paradoxical (REM) sleep. *Arch Ital Biol* **139**, 93–107.
Sakai K & Koyama Y (1996). Are there cholinergic and non-cholinergic paradoxical sleep-on neurones in the pons? *Neuroreport* **7**, 2449–2453.
Sakai K & Onoe H (1997). Critical role for M3 muscarinic receptors in paradoxical sleep generation in the cat. *Eur J Neurosci* **9**, 415–423.
Sakai K, Sastre JP, Kanamori N & Jouvet M (1981). State-specific neurones in the ponto-medullary reticular formation with specific reference to the postural atonia during paradoxical sleep in cat. In *Brain Mechanisms of Perceptual Awareness and Purposeful Behavior*, ed. Pompeiano M & Aimone Marsan C, pp. 405–429. Raven Press, New York.
Scammell TE (2003). The neurobiology, diagnosis, and treatment of narcolepsy. *Ann Neurol* **53**, 154–166.
Semba K (1993). Aminergic and cholinergic afferents to REM sleep induction regions of the pontine reticular formation in the rat. *J Comp Neurol* **330**, 543–556.
Shammah-Lagnado SJ, Negrao N, Silva BA & Ricardo JA (1987). Afferent connections of the nuclei reticularis pontis oralis and caudalis: a horseradish peroxidase study in the rat. *Neuroscience* **20**, 961–989.
Sheffler DJ, Williams R, Bridges TM, Xiang Z, Kane AS, Byun NE, Jadhav S, Mock MM, Zheng F, Lewis LM, Jones CK, Niswender CM, Weaver CD, Lindsley CW & Conn PJ (2009). A novel selective muscarinic acetylcholine receptor subtype 1 antagonist reduces seizures without impairing hippocampus-dependent learning. *Mol Pharmacol* **76**, 356–368.
Shen KZ & Johnson SW (2000). Presynaptic dopamine D_2 and muscarine M_3 receptors inhibit excitatory and inhibitory transmission to rat subthalamic neurones *in vitro*. *J Physiol* **525**, 331–341.
Soja PJ, López-Rodríguez F, Morales FR & Chase MH (1991). The postsynaptic inhibitory control of lumbar motoneurons during the atonia of active sleep: effect of strychnine on motoneuron properties. *J Neurosci* **11**, 2804–2811.
VanderHorst VG & Ulfhake B (2006). The organization of the brainstem and spinal cord of the mouse: relationships between monoaminergic, cholinergic, and spinal projection systems. *J Chem Neuroanat* **31**, 2–36.
Velazquez-Moctezuma J, Shalauta M, Gillin JC & Shiromani PJ (1991). Cholinergic antagonists and REM sleep generation. *Brain Res* **543**, 175–179.
Vetrivelan R, Chang C & Lu J (2011). Muscle tone regulation during REM sleep: neural circuitry and clinical significance. *Arch Ital Biol* **149**, 348–366.
Vetrivelan R, Fuller PM, Tong Q & Lu J (2009). Medullary circuitry regulating rapid eye movement sleep and motor atonia. *J Neurosci* **29**, 9361–9369.
Weber CR, Piacentino V 3rd, Ginsburg KS, Houser SR & Bers DM (2002). Na^+-Ca^{2+} exchange current and submembrane $[Ca^{2+}]$ during the cardiac action potential. *Circ Res* **90**, 182–189.
Xu C, Wu M, Morozova E & Alreja M (2006). Muscarine activates the sodium–calcium exchanger via M_3 receptors in basal forebrain neurons. *Eur J Neurosci* **24**, 2309–2313.

Additional Information

Competing interests

None declared.

Author contributions

Spinal cord injections and whole-cell recordings were performed by W.F.J., R.H.W. and J.M.H. Conception and design of experiments: W.F.J., R.H.W., J.L. and E.A. Data analysis and interpretation: W.F.J., R.H.W. and E.A. Manuscript writing: T.E.S., C.B.S. and E.A. All authors have approved the final version of the manuscript.

Funding

This study was supported by NIH grants: 1RO1NS061863, the Administrative Supplement Utilizing Recovery Act Funds 3RO1NS061863 and 1P01HL095491.

Acknowledgements

The authors wish to thank Sofia Z. Iqbal and Sarah A. Keating for assistance with animal surgeries and immunohistochemistry and Dr Patrick M. Fuller for his helpful comments on the manuscript.